MOX–Report No. 49/2014

Influence of the aortic valve leaflets on the fluid-dynamics in aorta in presence of a normally functioning bicuspid valve

D. Bonomi, C. Vergara, E. Faggiano, M. Stevanella, C. Conti, A. Redaelli, G. Puppini et al

MOX, Dipartimento di Matematica "F. Brioschi"
Politecnico di Milano, Via Bonardi 9 - 20133 Milano (Italy)

mox@mate.polimi.it http://mox.polimi.it

Influence of the aortic valve leaflets on the fluid-dynamics in aorta in presence of a normally functioning bicuspid valve

D. Bonomi[1], C. Vergara[2], E. Faggiano[1,3], M. Stevanella[4], C. Conti[5], A. Redaelli[4], G. Puppini[6], G. Faggian[7], L. Formaggia[1] and G.B. Luciani[7]

November 6, 2014

[1] MOX– Modellistica e Calcolo Scientifico, Dipartimento di Matematica, Politecnico di Milano, via Bonardi 9, 20133 Milano, Italy
diana.bonomi@polimi.it
[2] Dipartimento di Ingegneria Gestionale, dell'Informazione e della Produzione, Università di Bergamo, Italy
[3] LaBS, Dipartimento di Chimica, Materiali e Ingegneria Chimica, Politecnico di Milano, Italy
[4] Dipartimento di Elettronica, Informazione e Bioingegneria, Politecnico di Milano, Italy
[5] EnginSoft SpA, Parco Scientifico Tecnologico Kilometro Rosso, Bergamo, Italy
[6] Department of Radiology, Azienda Ospedaliera Universitaria Integrata di Verona, Polo Confortini, Verona, Italy
[7] Division of Cardiac Surgery, Department of Surgery, University of Verona, Italy

Keywords: Bicuspid aortic valve, aortic aneurysm, jet asymmetry, systolic helicoidal patterns

Abstract

In this work we consider the blood fluid-dynamics in the ascending aorta in presence of a normally functioning bicuspid aortic valve (BAV). In particular, we perform a computational study to assess the effect of the inclusion of the leaflets on the fluid-dynamic abnormalities characterizing BAV cases. Indeed, in previous works it has been shown that without leaflets it is possible to recover such abnormalities, in particular the strong systolic jet asymmetry, but it was not clear how the inclusion of the leaflets would have improve the results.

To this aim we perform a comparison in two real geometries (a dilated and a non-dilated ones) among three scenarios which are built up for each geometry: BAV without leaflets, BAV with leaflets, and tricuspid case (TAV) with leaflets. Our results show that the inclusion of the leaflets increases the fluid-dynamics abnormalities which are quantified through the introduction of suitable synthetic indices.

1 Introduction

Bicuspid aortic valves (BAV) provide in general a normally functioning regime in absence of other complications, such as regurgitation or aortic dissection. However, they are associated with an increased prevalence of ascending aortic dilatation and, possibly, aneurysm in comparison with a normally functioning tricuspid aortic valve (TAV) (Hahn et al, 1992; Fedak et al, 2002; Nkomo et al, 2003; Bauer et al, 2006). The reasons for this are matter of controversy: on the one hand it is believed that a genetic origin could lead to a weakening of the aortic wall (Siddiqi and M.D., 2014); on the other hand a crucial role seems to be played by the systolic blood fluid-dynamics observed in the ascending aorta in BAV cases (Barker and Markl, 2011; Girdauskas et al, 2011), where an abnormal fluid-dynamics has been described characterized by non-standard features in comparison with the one developed in a normally functioning TAV. In particular, the fluid-dynamics at systole in the ascending aorta in a normally functioning BAV feature:

1. An eccentric jet exiting from the left ventricle;
2. High concentrated wall shear stresses (WSS);
3. Elevated retrograde flows;
4. A possible helical flow, which becomes particularly intense in dilated cases.

These phenomena have been observed with medical imaging techniques, such as echocardiography (Schapira et al, 1979; Donal et al, 2005b) or phase-contrast magnetic resonance (PC-MRI) (Hope et al, 2014a, 2010; Den Reijer et al, 2010; Barker et al, 2010; Hope et al, 2011; Sigovan et al, 2011; Barker et al, 2012), with in-vitro experiments (Saikrishnan et al, 2012; Atkins et al, 2014) , and with computational models (Viscardi et al, 2010; Vergara et al, 2012; Della Corte et al, 2012; Chandra et al, 2012; Pasta et al, 2012; Faggiano et al, 2013). In particular, in (Faggiano et al, 2013) we observed that the four characteristics of the BAV fluid-dynamics mentioned above are not independent and are strictly related with one another. In (Viscardi et al, 2010; Vergara et al, 2012; Faggiano et al, 2013), rigid wall simulations where the valve orifice was projected on the valve plane (interface between left ventricle and aorta) and without modeling the leaflets were presented. These simulations highlighted that the shape and the area of BAV seem to be enough to reproduce the abnormal fluid-dynamics in the ascending aorta with a satisfying accuracy (see Faggiano et al (2013) for a quantitative comparison with 2D CINE PC-MRI data). However, in (Della Corte et al, 2012; Chandra et al, 2012; Marom et al, 2013b; Pasta et al, 2012) the importance of including the valve leaflets in the computational model has been highlighted to accurately describe the jet deflection and WSS.

In this paper we present a work aimed at investigating and quantifying the effect of the inclusion of the valve leaflets in fluid-dynamic numerical simulations

with rigid walls. In particular, we aimed at comparing BAV and TAV configurations in presence of the leaflets, and BAV configurations with and without leaflets. To this end, four indices measuring jet asymmetry, flow reversal, helical flow, and maximum wall shear stress were computed at the systole.

2 Methods

2.1 Data acquisition and generation of the volumes

In this work we considered two patient-specific non-stenotic BAV cases, one characterized by a normal ascending aorta (in what follows referred to as Patient 1), and the other one by a dilated ascending aorta with a diameter greater than 4cm (referred to as Patient 2). Both patients featured an antero-posterior (AP) orientation of the commissures. None of the patients was affected by additional structural diseases, including aortic coarctation or tetralogy of Fallot.

For both patients a 3D contrast enhanced MRI (CE-MRI) was acquired with a voxel resolution of $1.72 \times 1.72 \times 1.5$ mm. The following parameters were used: TE (Echo Time) = 1.02 ms; flip angle = 20 deg ; slice thickness = 1.5 mm; acquisition matrix = 256×106. The two geometries are shown in Figure 1. Two cross-sections are considered at two different aortic levels, namely the *sinotubular junction* and the *mid-ascending aorta*. We will refer to these sections as A1 and A2, respectively (see Figure 1).

Moreover, a breath-hold true fast imaging with steady state precession (True-Fisp) cine-sequence with retrogated ECG triggering was acquired on the valve plane, defined as the interface between the left ventricle and the aorta, with the following parameters: TE (Echo Time) = 1.6 ms; flip angle = 65 deg ; slice thickness = 8 mm; temporal resolution = 20 phases in one cardiac cycle; acquisition matrix = 256×146.

All the MRI acquisitions were performed on a 1.5 Tesla system (Magnetom Symphony, Siemens Medical Systems, Erlangen, Germany).

A surface model of the aortic root, ascending aorta and aortic arch of the two patients has been then generated from the 3D CE-MRI images, using a level-set segmentation technique implemented in the open-source code Vascular Modeling Toolkit (*vmtk*, `http://www.vmtk.org`). The surfaces have been then cut at the aortic valve planes and at the outlets, obtaining the starting volumes (see Figure 1).

2.2 Leaflets geometry

To include the leaflets in our geometries we preliminarily performed two structural simulations in a realistic but not specific geometry, one for a BAV and one for a TAV configuration. To this aim, finite element models of BAV and TAV configurations were based on average dimensions derived from 2D MRI acquisitions performed on 10 TAV and 8 AP-BAV subjects, respectively (Conti et al, 2010).

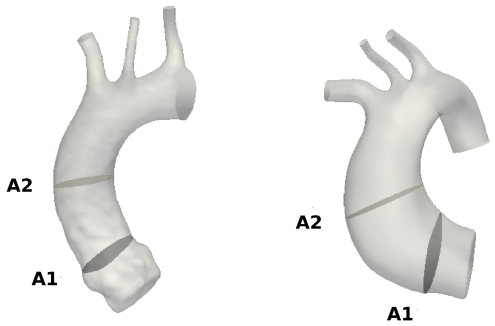

Figure 1: Computational domains. Left: Patient 1 with STJ (A1) and mid-ascending aorta (A2) sections; Right: Patient 2 with sections A1 and A2.

The mechanical response of aortic leaflets, modeled as a shell, was described via a transversely isotropic incompressible hyperelastic model, implemented into the ABAQUS/Explicit code (ABAQUS/ Explicit, SIMULIA Inc.) with a VUMAT subroutine, based on the following strain energy function (May-Newman and Yin, 1998):

$$W = c_0 \exp\left(c_1(I_1 - 3)^2 + c_2(I_4 - 1)^2 - 1\right), \tag{1}$$

where I_1 and I_4 are the first and fourth invariants of the Cauchy-Green strain tensor. Constants c_0, c_1, c_2 were set by fitting with the model reported by (Billiar and Sacks, 2000). Constitutive materials of the aorta were assumed linear, elastic and isotropic. The density was set equal to $1.1 g/mm^3$ for all tissues. A two-step simulation was performed on the model. First, the aortic root was pressurized by a linearly increasing load from the zero-pressure state to the tele-dyastolic aortic pressure level. Second, physiologic pressures were applied to the aortic root substructures. For further details we refer the reader to (Conti et al, 2010). This allowed to obtain two reference open leaflets configurations, one for BAV and one for TAV.

In this work we were interested in computing fluid-dynamic quantities at the systole, since they characterize the abnormal flow in presence of BAV. For this reason we considered the open configurations obtained by the BAV and TAV structural simulations in the reference geometry and we mapped them into the volumes of the two patients, using Gambit, an Ansys preprocessor for engineering analysis. This mapping has been realized for both patients imposing that the resulting dimension of the BAV orifices and the orientation of the valves were the same as those measured from the TrueFisp sequences. This allowed to obtain, for both Patients 1 and 2, a BAV and a TAV open leaflets configuration in the same volume, and then to appreciate the differences induced by the different valves, see Figure 2.

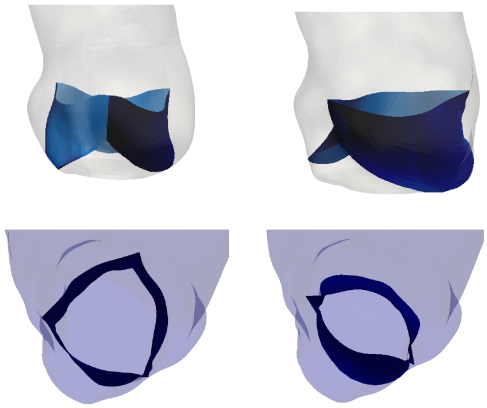

Figure 2: Valve leaflets for the tricuspid (left) and the bicuspid (right) configurations. Patient 1.

2.3 Generation of the meshes with the leaflets

Once we have obtained the four geometries with the open leaflets, we generated with *vmtk* a volume mesh of linear tetrahedra and a conforming superficial mesh for the leaflets, achieving for each of the two patients the computational domains with leaflets for the TAV and BAV cases. In what follows we refer to such meshes as BAV-leaflets and TAV-leaflets (see Figure 3, left, for the leaflets mesh).

All leaflets triangles were duplicated , thus obtaining two coinciding surfaces and a discontinuity of the solution through the leaflets.

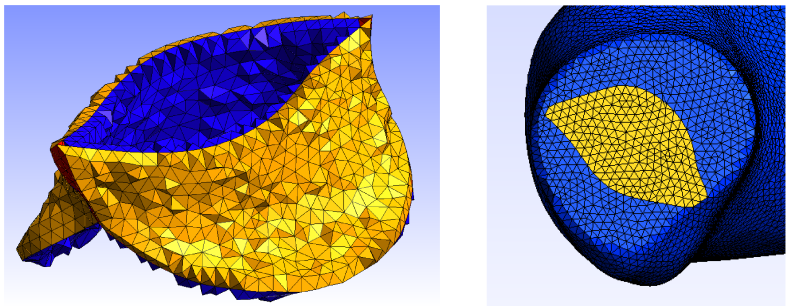

Figure 3: Mesh of the internal leaflets in the BAV configuration (left) and of the projected valve orifice (right).

2.4 Generation of the meshes without the leaflets

In order to assess the accuracy of the simulations in presence of the leaflets, we generated for the two BAV cases also the corresponding two meshes without leaflets. To this aim, we identified for each scenario the valve plane. Then, for both patients we projected onto the valve plane the orifice delimited by the endpoints of the leaflets in the systolic configuration. At the end, two regions were identified on this plane: the bicuspid valve orifice (light gray in Figure 3, right), which is the inlet for the fluid-dynamic simulations, and an impermeable region (dark grey in Figure 3, right). Then, a mesh of linear tetrahedra was generated with *vmtk* for each of the two patients, obtaining the computational domains without leaflets. In what follows we refer to such meshes as BAV-no-leaflets.

In Table 1 we report the values of the orifice area for all the meshes considered.

Concerning the number of elements of each mesh, we obtained about 600 000 tetrahedra and 120 000 vertices for all the meshes related to the Patient 1, about 750 000 tetrahedra and 140 000 vertices for the meshes related to the Patient 2.

	Patient 1	Patient 2
TAV-leaflets	3.1	4.2
BAV-leaflets	2.0	2.5
BAV-no-leaflets	1.8	2.3

Table 1: Values of the valve orifice areas expressed in cm^2.

2.5 Description of the numerical simulations

Unsteady numerical simulations were performed by using the finite element library LifeV (see `www.lifev.org`). Blood was considered as Newtonian, homogeneous, and incompressible, modeled by the Navier-Stokes equations for incompressible fluids (Formaggia et al, 2009). The blood viscosity was 0.035 Poise, the density was 1.0 g/cm3, and the time step was 0.01s. For time independence, we tested that doubling the time step or refining the meshes the results remained the same up to a suitable tolerance. We used P1-P1 finite elements stabilized with the Interior Penalty technique, see Burman et al (2006). The vessel wall was considered rigid since we do not expect that the dynamics of the wall substantially affects the abnormal systolic flows, especially the comparisons among the different cases. Being interested in the hemodynamics at systolic ejection, the opening and closure mechanism of the valve leaflets was not modeled in the case with leaflets, since we assumed that this would not influence the direction of the jet at systole and the other fluid-dynamic quantities. Valve opening and closure were therefore modeled in an on/off modality without considering the intermediate steps. For our tests we prescribed the same standard representative healthy

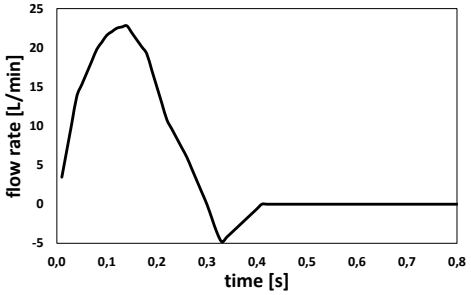

Figure 4: Representative flow rate curve imposed at the inlet in all the scenarios.

flow rate to both patients (Avolio, 1980) (see Figure 4). To prescribe this flow rate, a Dirichlet boundary condition at the inflow under the assumption of flat velocity profile was imposed (Moireau et al, 2012). At the outlets, a zero-stress condition was prescribed, since the region of interest is in the proximal ascending aorta. It must be highlighted that no turbulence models were assumed.

2.6 Indices for haemodynamic quantifications.

In order to perform a quantitative comparison among the various configurations, we introduced suitable easily computable indices providing useful information about the abnormal flow in the ascending aorta.

Flow asymmetry. BAV configurations lead to an asymmetric systolic flow in the ascending aorta. To quantify this eccentricity we used the normalized flow asymmetry index NFA proposed in (Sigovan et al, 2011), defined as follows:

$$NFA = \frac{||\mathbf{c}_S - \mathbf{c}_{vel}||}{L}, \tag{2}$$

where $\mathbf{c}_{vel}$ is the center of velocity on S defined as $(\mathbf{c}_{vel})_j = \frac{\int_S j\mathbf{u}^+ \cdot \mathbf{n} d\sigma}{\int_S \mathbf{u}^+ \cdot \mathbf{n} d\sigma}$, $j = x, y, z$, where $\mathbf{u}^+$ is the part of the velocity $\mathbf{u}$ such that $\mathbf{u}^+ \cdot \mathbf{n} > 0$ on S ($\mathbf{n}$ being the normal direction to the section S), $\mathbf{c}_S$ is the barycenter of the section S and L is a characteristic length of S.

We have $NFA = 0$ when the center of velocity lies in the center of the vessel (no asymmetric flow) and $NFA = 1$ when it is on the vessel wall (totally asymmetric flow).

Retrograde flow analysis. One of the features of the systolic abnormal flow induced by a BAV configuration is the formation of retrograde flows in the ascending aorta. To quantify them, we introduce the index FRR on a section,

defined as follows (Barker and Markl, 2011; Faggiano et al, 2013)

$$FRR = \frac{|Q_{neg}(t_{sys})|}{|Q_{pos}(t_{sys})|}\%, \tag{3}$$

where Q_{neg} and Q_{pos} represent the backward and forward flow rates on the section at hand, respectively and t_{sys} is the systolic instant. Observe that $FRR = 0$ means that no retrograde flow occurred.

Systolic helical flow pattern analysis. As observed in the Introduction, one of the peculiarity of the fluid-dynamics in BAV configurations, strictly related to the formation of retrograde flows and to the jet asymmetry, is the possible formation of helical structures in the ascending aorta at systole, which are completely absent in normal TAV configurations. To quantify such a phenomenon on a section S, in Faggiano et al (2013) we introduced the positive helix fraction index PHF defined as

$$PHF = \frac{H_{pos}}{H_{pos} + H_{neg}} \tag{4}$$

where $H_{pos} = \int_S h^+$, $H_{neg} = \int_S h^-$, h^+ and h^- are the positive and negative parts, respectively, of the quantity h, defined as

$$h = (\nabla \times ((\mathbf{u}(t_{sys}) \cdot \boldsymbol{\tau})\boldsymbol{\tau}) \cdot \mathbf{n}, \tag{5}$$

where $\boldsymbol{\tau}$ is the tangent direction to the surface S. h is nothing but the normal component of the systolic vorticity of the velocity parallel to the section S. PHF indicates the ratio between right-handed helices and the totality of the rotating flux ($PHF = 1$ means complete right-handed helical flow, $PHF = 0$ means complete left-handed helical flow, $PHF = 0.5$ means no prevalence of any direction).

Wall shear stresses. Strictly related to the formation of asymmetric flows is the production of elevated wall shear stresses in the ascending aorta. To quantify the wall shear stress we introduced the index $WSSmax$, which is the maximum of WSS evaluated on the ascending aorta (Faggiano et al, 2013).

3 Results

In this section we report the numerical results obtained for the different configurations we have presented. In the first part we analyze the velocity field and the values obtained for the indices proposed in Section 2.6. In the second part of the section we present the results of a parametric study obtained by varying the flow rate imposed at the inlet, in order to account for low flow rates often measured in BAV patients(Barker et al, 2012).

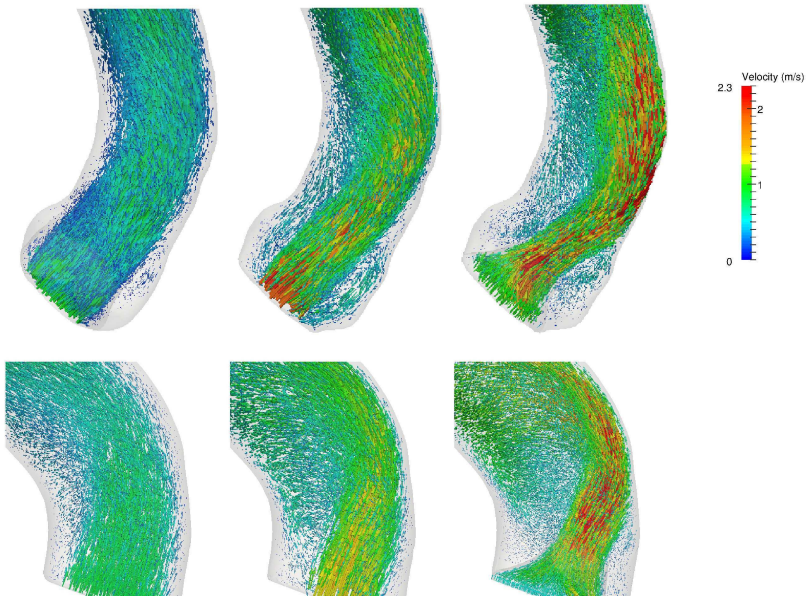

Figure 5: Velocity field at the systole for Patient 1 (top) and Patient 2 (bottom). From the left to the right: TAV-leaflets, BAV-no-leaflets, BAV-leaflets.

3.1 Quantification of the indices

3.1.1 Flow Asymmetry

In Figure 5 we show the flow pattern in the ascending aorta at the systole for the three different configurations BAV-leaflets, BAV-no-leaflets, TAV-leaflets for each patient.

From this figure we can see a remarkable difference in the fluid-dynamics between the TAV and the BAV cases, for both patients. We notice an asymmetric distribution of the velocity field in the BAV models, in particular between the valsalva sinus and the mid-ascending aorta, against a symmetric flow for the TAV configurations. In addition, BAV configurations feature higher values of the systolic velocity with respect to TAV. As for the comparison between the two BAV cases, with and without leaflets, we observe that the presence of the leaflets emphasizes the abnormal characteristic of the flow pattern leading to higher values of the velocity and to a more pronounced asymmetry in the ascending aorta for both patients.

In Table 2 the values of the NFA index for all the simulations are reported. We observe that the values obtained for TAV cases are very small, confirming the symmetry of the flow for patients with tricuspid aortic valve. On the contrary, in the BAV cases, the increased value of NFA highlights the deflection of the flow towards the wall, a phenomenon that increases approaching the mid-ascending aorta. In particular, we notice that at the STJ (section A1) there are differences

between the cases with and without leaflets of 17% for Patient 1 and 9% for Patient 2, whereas at the mid-ascending aorta (section A2) NFA values increase by 45% and 42% in the model with the leaflets. Finally, we observe that, in all configurations, the asymmetry is more pronounced for Patient 2, which is characterized by a dilated configuration of the ascending aorta.

	Patient 1		Patient 2	
	A1	A2	A1	A2
TAV-leaflets	0.080	0.076	0.175	0.077
BAV-no-leaflets	0.198	0.258	0.293	0.318
BAV-leaflets	0.232	0.375	0.318	0.451

Table 2: Values of the index NFA at the sinotubular junction (A1) and at the mid-ascending aorta (A2).

3.1.2 Retrograde flow

We report in Table 3 the values of the flow reversal ratio FRR for all the simulations. From these results we notice that in the TAV configurations there is no retrograde flow at the peak systole, FRR being very small at the STJ and exactly zero at the mid-ascending aorta. A clear increase of FRR in the bicuspid cases is observed. In particular, elevated values of the index occur in all BAV models at both levels A1 and A2, indicating the presence of a recirculation zone. This index features a behavior similar to that of NFA, in the sense that the differences between BAV models with and without leaflets are less pronounced at the STJ (A1) (an increment of 18% is observed in the case with leaflets for Patient 1 and of 10% in the case without leaflets for Patient 2). On the contrary, at the mid-ascending aorta (A2), the model without leaflets featured very small values of FRR (very close to zero, thus without any substantial retrograde flow), whereas the one with the leaflets experienced high values of FRR and thus a high retrograde flow.

	Patient 1		Patient 2	
	A1	A2	A1	A2
TAV-leaflets	0.28	0.0	4.49	0.0
BAV-no-leaflets	8.63	0.58	13.24	0.02
BAV-leaflets	10.19	9.69	11.80	10.36

Table 3: Values of the index FRR (in %) at the sinotubular junction (A1) and at the mid-ascending aorta (A2).

3.1.3 Helical flow analysis

Figure 6 shows the streamlines of the velocity field at the systole for Patient 2.

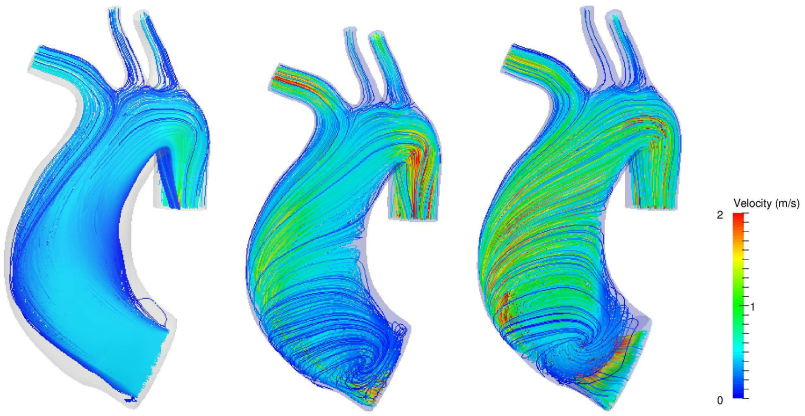

Figure 6: Streamlines of the velocity field at the systole for Patient 2. From the left to the right: TAV-leaflets, BAV-no-leaflets, BAV-leaflets.

We note a considerable difference between the TAV and the BAV cases. Indeed in the TAV configuration the flux goes straight into the ascending aorta, without creating any secondary flow. On the contrary in the BAV models the streamlines are not parallel to the wall and we can observe the formation of a vortex with an evident helical pattern (for the BAV-no-leaflets case see also Faggiano et al (2013)).

Figure 7 shows the velocity field and the quantity h at the level A2, highlighting the formation of a right-handed vortex for all BAV configurations (absent in the TAV-leaflets case), related to the lateral displacement of the flow and to its asymmetry. For each patient, the two BAV models, with and without leaflets, present comparable results and show the formation of very similar vortices, which however are slightly more pronounced in the BAV-leaflet configuration. In Table 4 we report the values of the PHF index at the mid-ascending aorta. These results confirm that the helical flow is absent for the TAV-leaflets cases (PHF very close to 0.5) and that it is more pronounced in the BAV case with leaflets. In particular, for the BAV cases PHF increased in the case with leaflets of 20% for Patient 1 and 15% for Patient 2. Moreover, they highlight the increased vorticity for Patient 2 with respect to Patient 1 for all the BAV cases. This suggests that the helical pattern is more relevant in case of aortic dilatation, thus confirming for the models with leaflets, what found for the case without leaflets in Faggiano et al (2013).

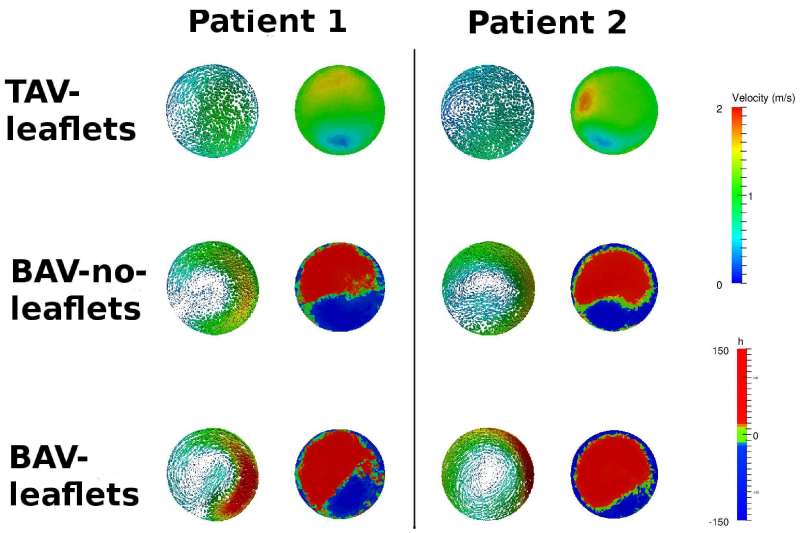

Figure 7: Top view of the mid-ascending aorta section (A2) with the computed three-dimensional velocity field and the corresponding h values for Patient 1 (left) and Patient 2 (right). From the top to the bottom: TAV-leaflets, BAV-no-leaflets, BAV-leaflets. h red colors stand for $h > 0$ (local right-handed helical structure), blue colors stand for $h < 0$ (local left-handed helical structure), and green colors stand for $h = 0$ (no local helical structure).

	Patient 1	Patient 2
TAV-leaflets	0.56	0.62
BAV-no-leaflets	0.61	0.73
BAV-leaflets	0.73	0.84

Table 4: Values of index PHF at the mid-ascending aorta (A2).

3.1.4 Wall shear stress

In Figure 8 we show the WSS for all the simulations performed. We observe a clear increase in the WSS values for all BAV configurations with respect to TAV-leaflets cases in the ascending aorta, where most of aortic aneurysms are located. The wall shear stress in this area is much higher than the values obtained for the TAV cases, where the distribution of the WSS is almost uniform. From a comparison between the two different BAV models we see that the leaflets lead to a considerable increase of the wall shear stress for both patients. In addition, we observe that, in presence of the leaflets, the area with higher values of WSS is located at a lower level with respect to the one obtained without leaflets.

Moreover, we report in Table 5 the values of the index $WSSmax$. These results confirm the qualitative observations made above. In particular, $WSSmax$

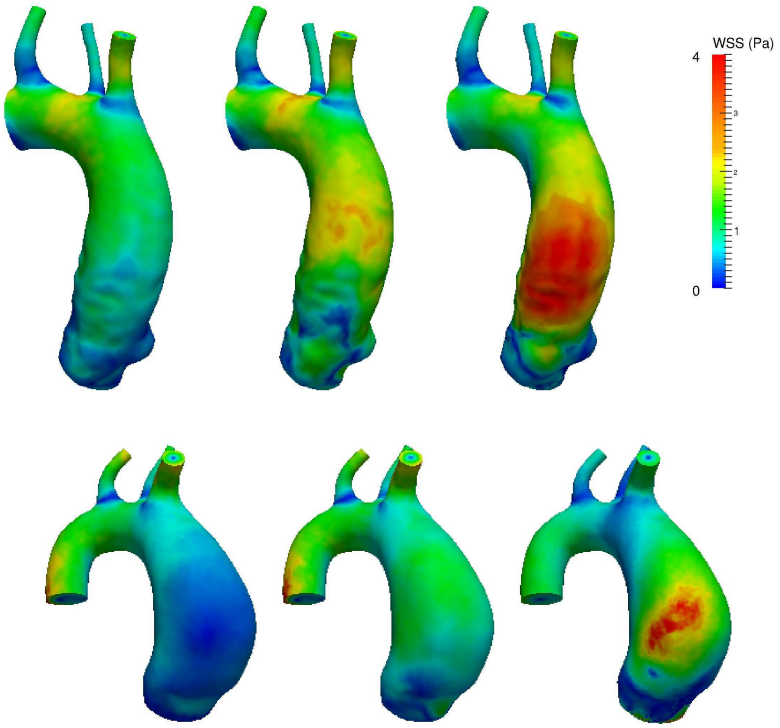

Figure 8: Wall shear stresses at the systole for Patient 1 (top) and Patient 2 (bottom). From the left to the right: TAV, BAV without leaflets, BAV with leaflets.

in the BAV-leaflets configurations is almost four time bigger than in the TAV-leaflets case and almost twice than in the BAV-no-leaflets configuration.

	Patient 1	Patient 2
TAV-leaflets	1.41	0.95
BAV-no-leaflets	2.42	1.73
BAV-leaflets	4.33	3.36

Table 5: Values of the index $WSSmax$.

3.2 Parametric flow rate analysis

Often, in BAV configurations the flow rate entering the aorta through the aortic valve is lower than the one occurring in a normal tricuspid case, because of recurring stenosis (Barker and Markl, 2011). In our cases, Patient 1 featured

a mild stenotic valve. This justified a sensitivity analysis to investigate the dependence of the proposed indices on maximum value of the flow rate. In particular, we performed the numerical simulations for all the BAV cases, by prescribing a flow rate at the inlet which is equivalent to $\frac{2}{3}$ of the previous ones, with a mean flow rate decreasing from 4,85 to 3,23 l/min. We refer to the standard and lower flow rates as $F1$ and $F2$, respectively.

In Tables 6, 7, 8, 9 we compare the values of the indices obtained with the original flow rates and with the reduced one, for both patients. We notice that the values of indices NFA and PHF related to the BAV model with the leaflets obtained with the lower flow rate $F2$ are in general very similar to those obtained with $F1$. On the contrary, we observe a marked difference among the results obtained with the two flow rates for the BAV-no-leaflets models, especially for NFA and PHF. In particular, in this case the abnormalities of the fluid-dynamics are strongly reduced with the lower flow rate, leading to a jet which is more symmetric and characterized by a small right-handed helical structure.

		Patient 1		Patient 2	
		A1	A2	A1	A2
F1	BAV-no-leaflets	0.198	0.258	0.293	0.318
	BAV-leaflets	0.232	0.375	0.318	0.451
F2	BAV-no-leaflets	0.080	0.131	0.188	0.190
	BAV-leaflets	0.226	0.361	0.336	0.481

Table 6: Values of index NFA at the STJ (A1) and at the mid-ascending aorta (A2). Flow rate parametric study.

		Patient 1		Patient 2	
		A1	A2	A1	A2
F1	BAV-no-leaflets	8.63	0.58	13.24	0.02
	BAV-leaflets	10.19	9.69	11.80	10.36
F2	BAV-no-leaflets	8.47	0.18	11.80	1.60
	BAV-leaflets	11.96	12.91	10.77	18.07

Table 7: Values of the index FRR at the STJ (A1) and at the mid-ascending aorta (A2). Flow rate parametric study.

		Patient 1	Patient 2
F1	BAV-no-leaflets	0.61	0.73
	BAV-leaflets	0.73	0.84
F2	BAV-no-leaflets	0.54	0.56
	BAV-leaflets	0.70	0.79

Table 8: Values of the index PHF at the mid-ascending aorta (A2). Flow rate parametric study.

		Patient 1	Patient 2
F1	BAV-no-leaflets	2.42	1.73
	BAV-leaflets	4.33	3.36
F2	BAV-no-leaflets	1.51	1.10
	BAV-leaflets	2.88	2.26

Table 9: Values of the the WSSmax index. Flow rate parametric study.

4 Discussion

4.1 State of the art and choice of the computational model

The study of the fluid-dynamics in the ascending aorta in presence of a bicuspid aortic valve by means of computational tools is a quite recent topic. To our knowledge, the first work in this direction has been provided by Richards et al (2004), where the authors considered 3D simulations in idealized rigid geometries, without any modelization of the leaflets. A similar investigation has been then provided in Donal et al (2005a). The first studies with patient-specific geometries have been reported in Viscardi et al (2010) and LaDisa et al (2010), where however the leaflets are not modeled and the valve orifice has been projected on the valve plane. Similar investigations have been then provided in Tse et al (2011), Vergara et al (2012) and Faggiano et al (2013). Other works considered the fluid-structure interaction arising between the blood and the aorta wall, we mention Weinberg and Kaazempur Mofrad (2008), Chandra et al (2012), and Marom et al (2013a) for the case of idealized geometries, and Pasta et al (2013) for patient-specific geometries. As for the modeling of the leaflets, to our knowledge the only works that considered them in the numerical simulations, either in rigid or compliant vessels, are Weinberg and Kaazempur Mofrad (2008), Della Corte et al (2012), Chandra et al (2012) and Marom et al (2013a) for idealized geometries, and Pasta et al (2013) for real geometries.

In this work we considered numerical simulations in patient-specific geometries with the presence of the leaflets, to assess the influence of the latter in the fluid-dynamics. In particular, we did not model the interaction between

the blood and the leaflets, instead we built two reference open configurations of the leaflets (one for TAV and one for BAV) by solving structural simulations based on the average of some patient-specific data, and then we mapped them into the patient-specific geometries. This choice has been done, as a first approximation, since here we were interested in simulating the fluid-dynamics at the systole, when the leaflets are completely open. Our aim was to perform a comparison with other configurations (BAV without leaflets, TAV with leaflets). In this respect, we believe that the complete opening/closure mechanism of the valve should not have a significant influence on the comparison of the systolic fluid-dynamic quantities. Moreover, we assumed a rigid aortic wall. Again, this simplifying hypothesis has been justified by observing that the description of the interaction between blood and vessel should not influence the comparison performed in this work.

4.2 Abnormal fluid-dynamics induced by a bicuspid configuration

As highlighted in the Introduction, the fluid-dynamics in the ascending aorta in presence of a non-stenotic bicuspid aortic valve is very different from the one developing in a TAV configuration. In particular, BAV configurations are characterized by a pronounced asymmetry of the systolic jet entering the aorta, which generates large zones of flow reversal, high WSS at the sino-tubular junction and mid-ascending aorta, and, often, systolic helicoidal patterns. The computational studies mentioned above described such abnormalities. In particular, the asymmetry of the jet has been firstly reported by the results in Donal et al (2005b), where however the authors prescribed a priori the angle between the jet direction and the longitudinal axis. Then, this phenomenon has been recovered without any a priori imposition on the jet angle by the results in Viscardi et al (2010), Tse et al (2011), Vergara et al (2012), Faggiano et al (2013), and Pasta et al (2013), for the case without leaflets, and in Della Corte et al (2012), Marom et al (2013a) and Chandra et al (2012) in presence of the leaflets. Moreover, in vivo evidences of flow asymmetry and sistolic helical flows has been reported in Barker et al (2012), Hope et al (2011). The abnormal maximum WSS in the ascending aorta has been reported by the results in Viscardi et al (2010) , LaDisa et al (2010), Tse et al (2011), and Pasta et al (2013), whereas the formation of flow reversals and systolic vortices in Tse et al (2011), Chandra et al (2012), Faggiano et al (2013), and Marom et al (2013a).

4.3 Comparison among different configurations

BAV-leaflets vs BAV-no-leaflets. The computational studies mentioned above suggested that the asymmetry of the systolic jet and the fluid-dynamic abnormalities observed in BAV configurations are provoked by two independent factors: i) The shape of the open BAV orifice in combination with the typical

curvature and torsion of the ascending aorta; ii) The presence of the BAV leaflets in the open configuration, which forces the jet direction.

In this work we tried to quantify these two separate contributions. To do this, we compared the numerical results obtained with and without the inclusion of the leaflets in BAV computational models. In particular, the comparison has been performed in two real geometries of the ascending aorta, a non-dilated one and a dilated one.

The results reported in Tables 2, 3, 4 and 5 showed that, for both patients, jet asymmetry, flow reversal, formation of helicoidal patterns and WSS increase at the systole when the leaflets are modeled. The increment of the indices quantifying the abnormal flow observed when the leaflets are included in the computational models could be explained by observing Figure 9. In particular, in this figure the systolic velocity field on a representative section located just below the plane given by the endpoints of the leaflets is reported for the BAV-leaflets configuration, together with the systolic velocity field on the same section obtained with the BAV-no-leaflets configuration. These plots highlight that the systolic jet is confined in a small region in the BAV-leaflets case due to the presence of the leaflets, whereas it is more spread out in the configuration without leaflets, since in this case the blood flowing between the valve orifice and the section at hand could diffuse in a wider region. This emphasizes the jet asymmetry (and thus the other abnormalities) in the case with leaflets at the STJ and, in particular, at the mid-ascending aorta level. This is in agreement with the fact that the inclusion of the leaflets produces a greater increment at the mid-ascending aorta with respect to the STJ for the NFA and FRR indices.

These results also suggest that the inclusion of the leaflets is important to describe the abnormal fluid-dynamics for BAV patients, especially for the non-dilated configuration (Patient 1), which presents a greater increment of the indices, see percentages reported in Sect. 3.1. Probably, the greater volume of the ascending aorta in the dilated case facilitates the formation of a pronounced jet asymmetry also without modelling the leaflets. This induces the formation of a vortex generated by the pressure difference occurring in the dilated region between the jet and the empty region. In the non dilated case, this dynamics is less pronounced and the inclusion of the leaflets becomes more influential for the generation of the jet asymmetry and of the other abnormalities.

BAV-leaflets vs TAV-leaflets. The comparison between the fluid-dynamics in BAV and TAV cases has been reported in several works. We mention Hope et al (2010, 2011); Barker and Markl (2011) among the radiological studies, Pasta et al (2013) as computational study in real geometries in presence of the leaflets, and Saikrishnan et al (2012) among the in-vitro studies.

Our results allowed to compare the fluid-dynamics in the TAV and in the BAV cases in presence of the leaflets, confirming the findings of the above works. In all the cases, the value of the indices increased notably in the BAV case. In

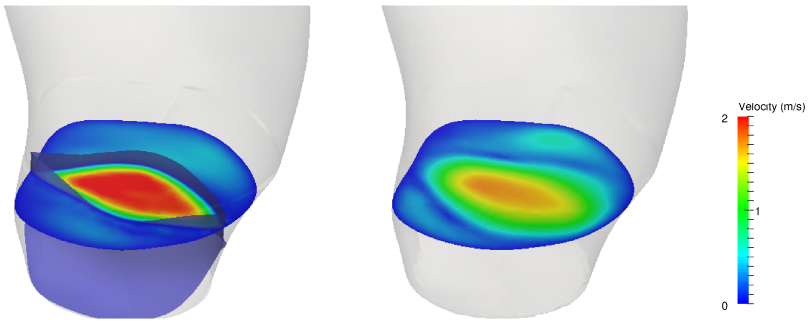

Figure 9: Velocity field on a selected section just below the endpoints of the leaflets in the BAV-leaflets configuration (left) and on the same section in the BAV-no-leaflets configuration (right).

particular, the NFA index was below 0.08 in the TAV-leaflets cases (except for a value of 0.175 at the STJ of Patient 2) supporting the thesis of a centered flow for TAV configurations also in presence of the leaflets. On the contrary, for the BAV-leaflets cases, it was always greater than 0.3 with a maximum of 0.45 at mid-ascending level of Patient 2. The FRR was almost always equal to 0.0% in TAV-leaflets cases with a peak of 4.49% at the STJ of Patient 2, whereas it assumed values around 10% in BAV-leaflets, demonstrating the appearance of retrograde flow only in BAV. The PHF assumed values near 0.5 in TAV-leaflets (absence of any prevalence between right and left handed flows), whereas it increased to 0.73 for Patient 1 and 0.83 for Patient 2 in BAV-leaflets cases, denoting a clear presence of a right handed flow. Also WSS values became at least three times greater in BAV-leaflets cases with respect to TAV-leaflets. These results highlighted that, also in presence of the leaflets, the fluid-dynamics in presence of BAV is very different from the one with TAV, which features a symmetric systolic jet, very low flow reversals, and no helicoidal patterns at the systole, thus confirming what found in previous works for the case without leaflets, see e.g. Vergara et al (2012).

Flow rate parametric study. Tables 6, 7, 8, 9 report the results obtained with a smaller flow rate prescribed at the inlet. This simulation has been carried out to define the influence of valve leaflets in presence of a reduced flow rate due for example to a mild aortic valve stenosis (as happens for Patient 1), a common situations for BAV patients. In fact, clinically relevant scenarios include patients with mildly or moderately stenotic BAV, with or without associated ascending aortic dilatation, either in natural history subject to follow-up imaging investigations or as result of surgical repair of regurgitant BAV (Luciani et al, 2012).

Passing from the original to the lower flow rate, NFA was nearly the same

in BAV-leaflets, whereas it decreased substantially in BAV-no-leaflets, assuming values similar to those of TAV-leafletes for the original flow rate; FRR increased in BAV-leaflets cases, whereas it remained nearly constant in BAV-no-leaflets with only one case in which it decreased; PHF, became nearly 0.5 for BAV-no-leaflets cases, indicating the loose of a prevalent helical structure, whereas in BAV-leaflets cases it decreased, however demonstrating a clear prevalence of a right handed helix; WSSmax decreased substantially for all the configurations, maintaining higher values (almost two times greater) in BAV-leaflets with respect to BAV-no-leaflets. From these results, we conclude that, in case of mild valve dysfunction only the shape of the valve orifice in combination with the particular geometry of the ascending aorta is not able to reproduce all the abnormalities of the fluid-dynamics. Thus, we recommend the inclusion of the leaflets in particular in presence of small flow rates.

4.4 Do leaflets provide more reliable results?

The results reported in this work for the BAV configurations highlighted a general tendency to have more pronounced fluid-dynamics abnormalities in the case where the leaflets are modelled with respect to the case where the valve orifice is projected on the valve plane and the leaflets are neglected. The question now is if leaflets inclusion gives more accurate results. Of course, our expectation is that the model with the leaflets should provide more reliable results, since the physical phenomenon is described in a more accurate way.

To support this observation, we report here very preliminary results about the comparison with measured data. In particular, we considered for Patient 2 a slice (called *PC-slice*) positioned at the mid-ascending aorta approximately at $2\,cm$ from the most distal part of the sinotubular junction, see Figure 10, left. On this slice we acquired a 2D CINE PC-MRI acquisition (see Appendix for more details). As inflow condition for the numerical simulations, we imposed the patient specific flow rate measured by the PC-MRI data (see Figure 10, right).

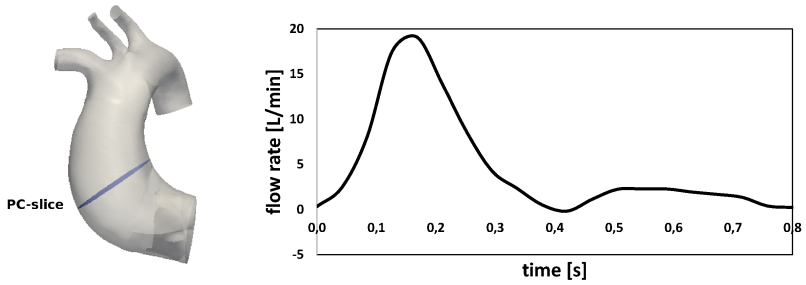

Figure 10: Location of the PC-slice for Patient 2 (left) and patient-specific inlet flow rate obtained by PC-MRI acquisitions (right).

In Figure 11 we show a top view of the PC-slice where the velocity field and

the h distribution are reported. We can see that both BAV models recognize the presence of a right handed vortex, showing a pattern that is, on a qualitative level, very similar to the measures, especially for the model with the leaflets.

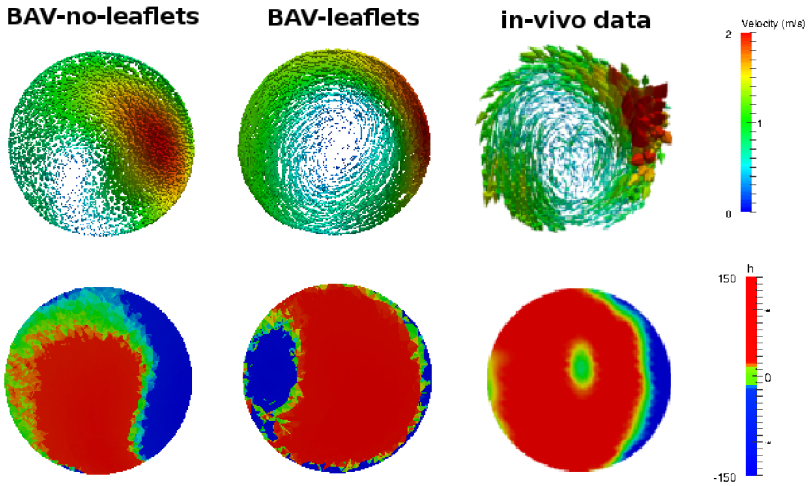

Figure 11: Velocity field (top row) and h distribution (bottom row) on the PC-slice. From left to right: BAV-no-leaflets, BAV-leaflets, in-vivo data.

In Table 10 we reported the values of NFA, FRR, and PHF obtained at the PC-slice with our BAV simulations and with the 2D CINE PC-MRI acquisition.

	NFA	FRR	PHF
BAV-no-leaflets	0.38	10.5	0.68
BAV-leaflets	0.53	22.2	0.82
In vivo	0.59	46.7	0.82

Table 10: Indices NFA, FRR, and PHF computed on the PC-slice.

These results showed that for all the indices there is a better agreement with the measures when the leaflets are modeled. In particular, NFA and PHF indices are almost identical, whereas FRR index is still far from the real value. This could be ascribed to two reasons: i) the absence in our models of the interaction with the aortic wall, producing a possible underestimation of the flow reversal due to the aortic dilatation; ii) the numerical dissipation which tends to soften the secondary flows. Since PHF index is in good agreement with the measures, we have a propensity to think that the main reason of the discrepancy observed for FRR index is due to the absence of a fluid-structure interaction model.

This comparison, although far to be a definitive validation, showed that the

increment observed for all the indices quantifying the fluid-dynamic abnormalities seems to be in the direction of a better description of the physical phenomena, thus providing a preliminary step towards a validation of our results.

5 Conclusions and Limitations

In previous work, it had been shown that the particular valve orifice shape in BAV configurations, in combination with the typical curvature and torsion of the aorta, was enough to reproduce the fluid-dynamic abnormalities absent in the TAV cases. In this paper, we showed that the inclusion of the leaflets in computational models canalizes the systolic jet, emphasizing the abnormalities of BAV flow, also in presence of failure. This has been proved by a preliminary validation with in-vivo data. In particular, we found that the inclusion of the leaflets is recommended to describe:

- Non-dilated ascending aortas;
- Cases with a reduced flow rate (as happens for stenotic BAV);
- Fluid-dynamic abnormalities at the mid-ascending aorta level.

The first limitation of this study concerns the clinical data acquired. Indeed, we did not have available the patient-specific configurations of the leaflets. Nowadays, with the modern image acquisition techniques it is possible to acquire this information, in particular for ad hoc studies. However, common clinical procedures often do not allow to have the adequate spatial and temporal resolution to detect the leaflets. Then, our work could provide concrete indications for those studies where no patient-specific leaflets are available.

Other limitations are related to the physical and computational models chosen for this study. First of all we made a rigid wall assumption, thus neglecting the interaction between fluid and aortic wall structure, and we did not consider an open/closure mechanism of the valve. As observed, this could be the cause of the significant underestimation of FRR index also in presence of the leaflets. Furthermore, we did not consider any turbulence or transition model, which is probably necessary in the ascending aorta (see Saikrishnan et al (2014) for an experimental study). In particular, the maximum Reynolds number characterizing our simulations was 4000 for Patient 1 and 5000 for Patient 2. As discussed, we do not believe that the inclusion of these features in our computations affects the final conclusions of the work, since this is a comparative study. However, the improvement of the physical and computational models will allow to obtain even more accurate indications about the fluid-dynamics in presence of BAV, so that we are working for future studies on these topics.

Appendix

We provide here some technical details on the 2D CINE PC-MRI acquisition made for Patient 2 at the PC-slice. A 1.5 Tesla system (Magnetom Symphony, Siemens Medical Systems, Erlangen, Germany) has been used. The temporal resolution was characterized by 20 phases in one cardiac cycle with a pixel resolution of 1.17×1.17 mm. Velocity encoding values were chosen to optimize the velocity map resolution with a value equal to 150 cm/s. The following parameters were also used: TE (Echo Time) = 6.4 ms; flip angle = 15 deg; slice thickness = 5 mm; acquisition matrix = 256×256.

References

Atkins S, Cao K, Rajamannan N, Sucosky P (2014) Bicuspid aortic valve hemodynamics induces abnormal medial remodeling in the convexity of porcine ascending aortas. Biomechanics and Modeling in Mechanobiology 13(6):1–17,

Avolio P (1980) Multi-branched model of the human arterial system. Medical & biological engineering & computing 18(6):709–18,

Barker A, Markl M (2011) Editorial: the role of hemodynamics in bicuspid aortic valve disease. Eur J Cardio-thorac Surg 39(6):805–806

Barker A, Lanning C, Shandas R (2010) Quantification of hemodynamic wall shear stress in patients with bicuspid aortic valve using phase-contrast mri. Annals of Biomedical Engineering 38(3):788–800

Barker A, Markl M, BÃijrk J, Lorenz R, Bock J, Bauer S, Schulz-Menger J, Von Knobelsdorff-Brenkenhoff F (2012) Bicuspid aortic valve is associated with altered wall shear stress in the ascending aorta. Circulation: Cardiovascular Imaging 5(4):457–466

Bauer M, Siniawski H, Pasic M, Schaumann B, Hetzer R (2006) Different hemodynamic stress of the ascending aorta wall in patients with bicuspid and tricuspid aortic valve. Journal of Cardiac Surgery 21(3):218–220

Billiar K, Sacks M (2000) Biaxial mechanical properties of the natural and glutaraldehyde treated aortic valve cusp - part i: Experimental results. Journal of Biomechanical Engineering 122(1):23–30

Burman E, Fernandez M, Hansbo P (2006) Continuous interior penalty finite element method for oseen's equations. SIAM Journal on Numerical Analysis 44(3):1248–1274

Chandra S, Rajamannan N, Sucosky P (2012) Computational assessment of bicuspid aortic valve wall-shear stress: Implications for calcific aortic valve disease. Biomechanics and Modeling in Mechanobiology 11(7):1085–1096

Conti C, Della Corte A, Votta E, Del Viscovo L, Bancone C, De Santo L, Redaelli A (2010) Biomechanical implications of the congenital bicuspid aortic valve: a finite element study of aortic root function from in vivo data. Journal of Thoracic and Cardiovascular Surgery 140(4):890–896

Della Corte A, Bancone C, Conti C, Votta E, Redaelli A, Del Viscovo L, Cotrufo M (2012) Restricted cusp motion in right-left type of bicuspid aortic valves: A new risk marker for aortopathy. Journal of Thoracic and Cardiovascular Surgery 144(2):360–369

Den Reijer P, Sallee D, Van Der Velden P, Zaaijer E, Parks W, Ramamurthy S, Robbie T, Donati G, Lamphier C, Beekman R, Brummer M (2010) Hemodynamic predictors of aortic dilatation in bicuspid aortic valve by velocity-encoded cardiovascular magnetic resonance. Journal of Cardiovascular Magnetic Resonance 12(1) DOI 10.1186/1532-429X-12-4

Donal E, Novaro G, Deserrano D, Popovic Z, Greenberg N, Richards K, Thomas J, Garcia M (2005a) Planimetric assessment of anatomic valve area overestimates effective orifice area in bicuspid aortic stenosis. Journal of the American Society of Echocardiography 18(12):1392–1398

Donal E, Raud-Raynier P, Coisne D, Allal J, Herpin D (2005b) Tissue doppler echocardiographic quantification. comparison to coronary angiography results in acute coronary syndrome patients. Cardiovascular Ultrasound 3(10):1–9

Faggiano E, Antiga L, Puppini G, Quarteroni A, Luciani G, Vergara C (2013) Helical flows and asymmetry of blood jet in dilated ascending aorta with normally functioning bicuspid valve. Biomechanics and Modeling in Mechanobiology 12(4):801–813

Fedak P, Verma S, David T, Leask R, Weisel R, Butany J (2002) Clinical and pathophysiological implications of a bicuspid aortic valve. Circulation 106(8):900–904

Formaggia L, Quarteroni A, Veneziani A (2009) Cardiovascular Mathematics, Modeling and simulation of the circulatory system, vol 1. Springer

Girdauskas E, Borger M, Secknus M, Girdauskas G, Kuntze T (2011) Is aortopathy in bicuspid aortic valve disease a congenital defect or a result of abnormal hemodynamics? a critical reappraisal of a one-sided argument. Eur J Cardiothorac Surg 39(6):809–815

Girdauskas E, Disha K, Borger MA, Kuntze T (2012) Relation of bicuspid aortic valve morphology to the dilatation pattern of the proximal aorta: Focus on the transvalvular flow. Cardiology Research and Practice DOI 10.1155/2012/478259

Hahn R, Roman M, Mograder A, Devereux R (1992) Association of aortic dilation with regurgitant, stenotic and functionally normal bicuspid aortic valves. Journal of the American College of Cardiology 19(2):283–288

Hope M, Hope T, Meadows A, Ordovas K, Urbania T, Alley M, Higgins C (2010) Bicuspid aortic valve: four-dimensional mr evaluation of ascending aortic systolic flow patterns. Radiology 255(1):53–61

Hope M, Hope T, Crook S, Ordovas K, Urbania T, Alley M, Higgins C (2011) 4d flow cmr in assessment of valve-related ascending aortic disease. JACC: Cardiovascular Imaging 4(7):781–787

Hope M, Sigovan M, Wrenn S, Saloner D, Dyverfeldt P (2014a) Mri hemodynamic markers of progressive bicuspid aortic valve-related aortic disease. Journal of Magnetic Resonance Imaging 40(1):140–145

Hope MD, Sigovan M, Wrenn SJ, Saloner D, Dyverfeldt P (2014b) Mri hemodynamic markers of progressive bicuspid aortic valve-related aortic disease. Journal of Magnetic Resonance Imaging 40(1):140–145

LaDisa J, Taylor C, Feinstein J (2010) Aortic coarctation: Recent developments in experimental and computational methods to assess treatments for this simple condition. Progress in Pediatric Cardiology 30(1-2):45–49

Luciani G, De Rita F, Lucchese G, Hila D, Rungatscher A, Faggian G, Mazzucco A (2012) Repair of congenitally dysplastic aortic valve by bicuspidization: Midterm results. Annals of Thoracic Surgery 94(4):1173–1179

Marom G, Haj-Ali R, Rosenfeld M, SchÃd'fers H, Raanani E (2013a) Aortic root numeric model: Annulus diameter prediction of effective height and coaptation in post-aortic valve repair. Journal of Thoracic and Cardiovascular Surgery 145(2):406–411

Marom G, Kim HS, Rosenfeld M, Raanani E, Haj-Ali R (2013b) Fully coupled fluid-structure interaction model of congenital bicuspid aortic valves: Effect of asymmetry on hemodynamics. Medical and Biological Engineering and Computing 51(8):839–848

May-Newman K, Yin F (1998) A constitutive law for mitral valve tissue. Journal of Biomechanical Engineering 120(1):38–47

Moireau P, Xiao N, Astorino M, Figueroa C, Chapelle D, Taylor C, Gerbeau JF (2012) External tissue support and fluid-structure simulation in blood flows. Biomechanics and Modeling in Mechanobiology 11(1-2):1–18

Nkomo V, Enriquez-Sarano M, Ammash N, Melton L, Bailey K, Desjardins V, Horn R, Tajik A (2003) Bicuspid aortic valve associated with aortic dilatation. Arteriosclerosis Thromb Vasc Biol 23(2):351–356

Pasta S, Phillippi J, Gleason T, Vorp D (2012) Effect of aneurysm on the mechanical dissection properties of the human ascending thoracic aorta. Journal of Thoracic and Cardiovascular Surgery 143(2):460–467

Pasta S, Rinaudo A, Luca A, Pilato M, Scardulla C, Gleason T, Vorp D (2013) Difference in hemodynamic and wall stress of ascending thoracic aortic aneurysms with bicuspid and tricuspid aortic valve. Journal of Biomechanics 46(10):1729–1738

Saikrishnan N, Yap C, Milligan N, Vasilyev N, Yoganathan A (2012) In vitro characterization of bicuspid aortic valve hemodynamics using particle image velocimetry. Annals of Biomedical Engineering 40:1760–1775

Saikrishnan N, Mirabella L, Yoganathan A (2014) Bicuspid aortic valves are associated with increased wall and turbulence shear stress levels compared to trileaflet aortic valves. Biomechanics and Modeling in Mechanobiology DOI 10.1007/s10237-014-0623-3

Schapira J, Martin R, Fowles R (1979) Two dimensional echocardiographic assessment of patients with bioprosthetic valves. The American Journal of Cardiology 43(3):510–519

Siddiqi K, MD K (2014) The aortopathy of bicuspid aortic valves. Controversies in Aortic Dissection and Aneurysmal Disease 49–65

Sigovan M, Hope M, Dyverfeldt P, Saloner D (2011) Comparison of four-dimensional flow parameters for quantification of flow eccentricity in the ascending aorta. Journal of Magnetic Resonance Imaging 34(5):1226–1230

Tse K, Chiu P, Lee H, Ho P (2011) Investigation of hemodynamics in the development of dissecting aneurysm within patient-specific dissecting aneurismal aortas using computational fluid dynamics (cfd) simulations. Journal of Biomechanics 44(5):827–836

Vergara C, Viscardi F, Antiga L, Luciani G (2012) Influence of bicuspid valve geometry on ascending aortic fluid dynamics: A parametric study. Artificial Organs 36(4):368–378

Viscardi F, Vergara C, Antiga L, Merelli S, Veneziani A, Puppini G, Faggian G, Mazzucco A, Luciani G (2010) Comparative finite element model analysis of ascending aortic flow in bicuspid and tricuspid aortic valve. Artificial Organs 34(12):1114–1120

Weinberg E, Kaazempur Mofrad M (2008) A multiscale computational comparison of the bicuspid and tricuspid aortic valves in relation to calcific aortic stenosis. Journal of Biomechanics 41(16):3482–348

MOX Technical Reports, last issues

Dipartimento di Matematica "F. Brioschi",
Politecnico di Milano, Via Bonardi 9 - 20133 Milano (Italy)

49/2014 D. Bonomi, C. Vergara, E. Faggiano, M. Stevanella, C. Conti, A. Redaelli, G. Puppini et al
Influence of the aortic valve leaflets on the fluid-dynamics in aorta in presence of a normally functioning bicuspid valve

48/2014 Penta, R; Ambrosi, D; Shipley, R.
Effective governing equations for poroelastic growing media

47/2014 Penta, R; Ambrosi, D; Quarteroni, A.
Multiscale homogenization for fluid and drug transport in vascularized malignant tissues

46/2014 Penta, R; Ambrosi, D.
The role of the microvascular tortuosity in tumor transport phenomena

45/2014 Pezzuto, S.; Ambrosi,D.; Quarteroni, A.
An orthotropic active-strain model for the myocardium mechanics and its numerical approximation

44/2014 Pezzuto, S.; Ambrosi,D.
Active contraction of the cardiac ventricle and distortion of the microstructural architecture

43/2014 Brugiapaglia, S.; Micheletti, S.; Perotto, S.
Compressed solving: a numerical approximation technique for PDEs based on compressed sensing

42/2014 Canale, A.; Vantini, S.
Constrained Functional Time Series: an Application to Demand and Supply Curves in the Italian Natural Gas Balancing Platform

41/2014 Esfandiar, B.; Porta, G.; Perotto, S.; Guadagnini, A.
Impact of space-time mesh adaptation on solute transport modeling in porous media

40/2014 Antonietti, P.F.; Mazzieri, I.; Quarteroni, A.
Improving seismic risk protection through mathematical modeling